Robot Hand based on a Spherical Parallel Mechanism for Within-Hand Rotations about a Fixed Point

Vatsal V. Patel, *Student Member*, IEEE, and Aaron M. Dollar, *Senior Member,* IEEE

***Abstract*—Rotating a grasped object about all three spatial axes is challenging, because kinematically redundant robot hands require complex control schemes for within-hand rotations, and simple parallel grippers require inefficient whole arm motions. We present a novel 3-finger robot hand design inspired by a spherical parallel mechanism that achieves these rotations with just 3 actuators. The hand is designed such that at every hand-object configuration, the object pose moves along a sphere with a fixed center, which is determined by the intersection of the fingers' revolute axes and is independent of the object shape, pose, and the initial grasp configuration. We optimize the hand based on 3-RRS spherical manipulator to maximize both its rotational workspace size and manipulation motion quality. From these parameters, we implement and experimentally evaluate the hand design through grasping tests, manipulation characterization, and real-world task scenarios, which show that the hand is able to grasp a variety of object geometries and accomplish precise single and multi-DOF rotations about a fixed point. We believe this design can remarkably improve robustness and simplify control for dexterous within-hand rotations, which finds utility in augmenting the capabilities of low-DOF robot arms without an active wrist.**

Index terms—Dexterous Manipulation, Mechanism Design, In-Hand Manipulation, Grasping, Parallel Robots

I. Introduction

The hand plays an integral role in functional robot manipulation by physically interacting with the robot's environment. While a simple gripper on a standard 6-7 degree of freedom (DOF) robot arm may be sufficient for many constrained applications like manufacturing, a dexterous end effector capable of precisely reorienting and repositioning grasped objects can be critical in overcoming practical shortcomings such as avoiding obstacles and arm singularities, improving safety and speed, and increasing energy efficiency [1]. In-hand manipulation of this nature has been previously achieved through anthropomorphic hand designs with serial, fully actuated fingers that often require accurate knowledge of object shape and contact locations for their complex redundant control schemes [2]–[5].

Traditional hand designs struggle in particular at within-hand object rotations where out-of-plane finger deflection is essential, because the flexion of revolute joints in these designs is primarily constrained to the plane of the finger. Researchers have evaluated actuated rotary and roller finger pads to enable such reorientation of the grasped objects [6], [7]. Another

This work was supported by the United States National Science Foundation under Grant IIS-1734190.

V. V. Patel, and A. M. Dollar are with the Department of Mechanical Engineering and Materials Science, Yale University, USA ({V.Patel, Aaron.Dollar}@yale.edu).

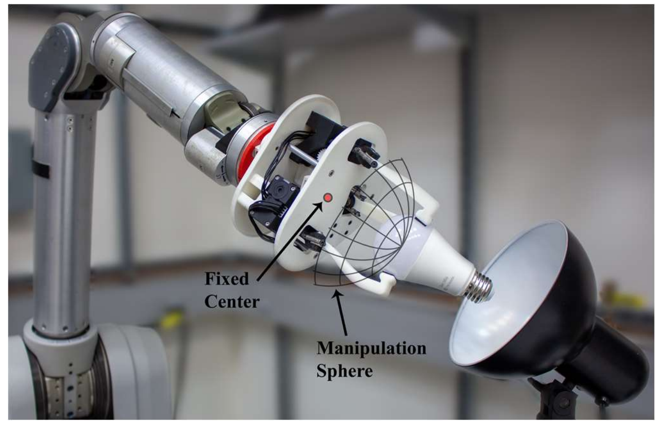

Fig. 1. Prototype of the 3-finger hand architecture based on the 3-RRS spherical parallel mechanism that can manipulate grasped objects in all rotational DOFs with 3 actuators, while the object centroid moves on a sphere with a fixed center. The center is invariant to object geometry or pose, and is determined by the intersection of the fingers' revolute axes.

common approach to within-hand yaw rotations (along axis perpendicular to palm) has been regrasping and finger-gaiting [8], [9]. An active wrist joint on the robot arm can speed up these yaw rotations, but can also result in undesirable panning and translation of the object if the wrist axis does not intersect on the object. To ensure predictable rotations about a known point, surgical robots utilize a fixed purely kinematic remote center of motion for manipulating their instruments [10].

The spherical hand topology introduced in [11] featured curved fingers with spatial flexion motion profiles and attempted to simplify planning of dexterous object manipulation by reducing the reliance on accurate object and contact modeling. The instantaneous revolute axes on the curved fingers of the hand intersected at a fixed point, about which the grasped object was expected to move. A caveat to this design was that the fingers' out-of-plane free-swing trajectory was unable to generate sufficient grasping forces, and the resulting achievable workspace with a passive pivoting thumb was not entirely spherical. The spherical hand concept did, however, introduce intersection of screw axes as novel hand topologies that made passive reconfiguration in underactuated hands more predictable.

Parallel robot manipulators offer another simple design architecture without the kinematic redundancies, since such mechanisms often have a single actuator per leg and per DOF of the movable platform. An equivalence can be drawn between the robot hand-object system during within-hand manipulation, and the closed kinematic chain created by the legs of a parallel platform—the palm corresponds to the fixed platform base, and the grasped object to the movable platform. Prior work has utilized the parallel robot analog to analyze within-hand manipulation [12], and some works have even implemented parallel mechanisms in their hand designs—the Metahand incorporates a spherical parallel mechanism into an articulated palm [13], [14], and McCann et al. present a hand design inspired by the 6-DOF Stewart-Gough parallel platform mechanism [15].

We explore spherical parallel mechanisms as a strategy to supplement parallel mechanism-based hand designs with in-hand rotation capabilities about a known fixed point [16]–[24]. The resulting object workspace of this hand architecture does not need to be experimentally validated through an exhaustive search of the actuation space, because any finite motion of the grasped object reduces to a spherical rotation about the point of convergence of the joint axes. Spherical parallel mechanisms thus generate an invariant manipulation space that is independent of the object shape, initial grasp, and the system's internal forces or pose. The purely kinematic nature of the mechanism's constraints is also highly desirable for its performance repeatability and robustness to operational errors.

To the authors' knowledge, apart from [11] no other hand designs have yet been explored for within-hand manipulation about a fixed point. Whereas, several spherical parallel architectures have been extensively studied to accomplish this type of motion with their movable platforms. So, in this work, we present a novel 3-fingered robot hand (Fig. 1) inspired by a spherical parallel mechanism to achieve within-hand rotations about a fixed center in all 3 DOFs with 3 actuators. The rest of the paper is organized as follows: Section II describes the 3-RRS spherical parallel mechanism that the hand architecture is based on, Section III presents an optimization framework to maximize performance from the mechanism, Section IV details the mechanical design of a physical prototype implemented with the optimal parameters, Section V outlines the experimental results from grasping tests, manipulation characterization, and real-world tasks performed with the prototype hand, and finally, Section VI summarizes the results and discusses future work to further augment the hand's capabilities.

II. 3-RRS Spherical Parallel Mechanism

The proposed hand architecture was inspired by the 3-$\underline{R}$RS spherical parallel mechanism [25]–[27], wherein each of the 3 legs are identical and comprised of 1 actuated revolute ($\underline{R}$) joint, 1 passive revolute (R) joint, and 1 passive spherical (S) joint. All 6 revolute axes intersect at a common point, and the motion of the platform is on a sphere with this fixed common point as its center, thus qualifying such an architecture as a spherical parallel mechanism. The 3-$\underline{R}$RS mechanisms do not inherently have this property if their axes do not converge at one point [28], [29]. And, conversely, spherical parallel mechanisms can be generated using several different architecture types such as with equal legs [16]–[18], with base and platform connected via spherical joints [19], [20], and several other non-overconstrained architectures [21]–[24]. The 3-$\underline{R}$RS spherical parallel platform architecture specifically also has the benefit of not being overconstrained—the mobility of the 3-$\underline{R}$RS closed kinematic chain is 3 from the Chebychev–Grübler–Kutzbach criterion [30], same as the number of actuators. This is particularly important when adapting the mechanism to a hand design, since it avoids control complexities that stem from the requirement to coordinate all joints in order to maintain a stable grasp during manipulation.

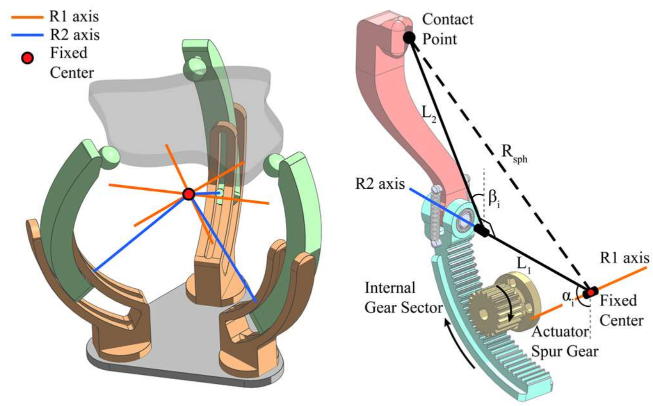

(a) (b)

Fig. 2. (a) Simplified illustration of the 3-RRS spherical parallel platform as a hand with all revolute joint axes intersecting at the fixed center, and the spherical joint estimated as a point contact with friction. (b) Design parameters and physical implementation of the fingers (equivalently, legs of the parallel platform).

In developing a hand architecture based on the 3-$\underline{R}$RS spherical parallel mechanism, the object would substitute the movable platform and would be grasped with rigid fingertips modeled as point contacts with friction. The spherical joint between the leg and movable platform is kinematically equivalent to this contact model [31], and thus the grasped object would still be manipulated about the same fixed point. A friction and normal force requirement (discussed in detail in Section III) for contact forces at the fingertip needs to be added to maintain grasp stability, completing the transformation of the spherical joint of the parallel mechanism. The revolute joints can be adapted without any change, and the resulting adapted hand based on the 3-$\underline{R}$RS spherical parallel platform architecture is shown in Fig. 2 (a). Since the complete hand-object system retains the kinematic constraints of its parallel platform equivalent, singularity analysis and inverse kinematic solutions can be derived from the parallel platform too. These are solved for in [25], and are not included here for brevity. The non-linear inverse kinematics result in 2 possible solutions per leg of the platform. But this is resolved by accounting for joint limits that would be present in any physical implementation of this hand design. The singularities of the parallel platform are addressed by looking at a transmission index metric also detailed in the following section.

III. Design Optimization

Parallel robots can be significantly improved from their initial design with careful parameter optimization [32], [33]. We determine two main characteristics that the performance of this hand architecture depends on—size of the rotational workspace considering the frictional contact constraints, and motion quality due to presence of singularities that could prevent the object from being manipulated through the said workspace. First, critical design parameters and their search space constraints need to be identified, which can then be optimized to generate a design with the best metrics for both characteristics. The overall size of the hand is determined by the radius of the sphere (R_{sph}) that the contacts lie on, so this can be used to non-dimensionalize the link lengths. Note that the center of this sphere that the contacts move on is also at the same intersection point of the revolute axes. To limit the search space size, we require link lengths to be identical across the 3 fingers, and the axes of rotation of the R1 joints (Fig. 2) to be parallel to the base of the hand. The latter constraint also prevents complex design accommodations that would be needed to accurately mount the actuators at different angles, so that the axes still converge at one common point. Lastly, in order to grasp the widest variety of object shapes, we require the contact points to be equidistant from each other (i.e., form an equilateral triangle) when grasping an object of diameter equal to R_{sph}. If this object diameter is not pre-specified, the R2 joint would have to be actuated in order to maintain an equilateral contact triangle during free swing motion of the fingers. Note that other object shapes can still be grasped and manipulated, but the grasp triangle would not be exactly equilateral.

Following the constraints established on the parameter search space, the framework needs to optimize the following parameters—link 1 length (L_1), and initial angle of the R2 joint ($\beta_{init,i}$ for i^{th} finger) as shown in Fig. 2 (b)—to maximize metrics on grasp stable workspace size, and motion quality within that workspace. The parameter search space and the respective metrics optimized are shown in Table 1. In the following analysis, we observe that these 2 parameters are largely decoupled in how they impact the 2 performance characteristics i.e., each parameter can be separately optimized to maximize one criterion without much effect on the other.

TABLE 1. OPTIMIZATION DESIGN PARAMETERS RANGES AND VALUES.

Symbol	Quantity	Range	Optimization Metric	Optimal Value
L_1/R_{sph}	normalized link 1 length	[0.05,0.95] 19 steps	size of grasp stable workspace	$\mathbf{0.5}$
$\begin{bmatrix}\beta_{init,1}\\ \beta_{init,2}\\ \beta_{init,3}\end{bmatrix}$	initial angle of R2 joint at the 3 fingers	$[-25°, 25°]$ 11 steps	motion quality (avg. TI_{hand} over workspace)	$\begin{bmatrix}\mathbf{20°}\\ \mathbf{-5°}\\ \mathbf{-5°}\end{bmatrix}$

A. Size of Grasp Stable Workspace

In adapting from the parallel mechanism to a hand-object system, the hand adds a frictional contact constraint so as to maintain sufficient grasp forces when manipulating an object. This constraint is checked by evaluating if the contact force at a fingertip falls within its friction cone. First, the desired object pose must fall within the workspace determined by the kinematic limits of the hand. These are established from the inverse kinematics model of the parallel platform in [25] along with joint limit considerations for a physical implementation. Then, the contact grasp forces at the fingertips for the desired object pose must also satisfy aforementioned frictional limits so that a stable grasp can be maintained. We adopt the methodology from [34] to determine if contact forces are within the friction cone at fingertips for a given object pose.

The computational model of the hand-object system to predict whether a particular object pose is stable builds on the criteria in [35] that relates the contact forces f_c to the 6-DOF external wrench F_e acting on the object through the grasp matrix $\mathbf{G} \in \mathbb{R}^{6\times 3n}$ for n point contacts with friction.

$$\mathbf{G}f_c = -F_e \tag{1}$$

In this study, the weight of the object was used as the applied external wrench. For our 3-fingered hand, the system of equations does not uniquely compute the contact force vector ($f_c \in \mathbb{R}^{9\times 1}$) for some external wrench ($F_e \in \mathbb{R}^{6\times 1}$). However, a component of the reaction force at the contacts is due to the force applied by the actuators, and thus provides 3 additional equations for the previously rank-deficient system of equations. Assuming the actuators each apply a grasping torque τ_g at the base of the finger, and the moment arm from the actuator axis to the contact point is r_i for the i^{th} finger, the augmented grasp matrix $\mathbf{G_{aug}} \in \mathbb{R}^{9\times 9}$ can now uniquely solve for the contact forces f_c.

$$\mathbf{G_{aug}}f_c = \begin{bmatrix}-F_e\\ \tau_g r_1\\ \tau_g r_2\\ \tau_g r_3\end{bmatrix} \rightarrow f_c = \mathbf{G_{aug}}^{-1}\begin{bmatrix}-F_e\\ \tau_g r_1\\ \tau_g r_2\\ \tau_g r_3\end{bmatrix} \tag{2}$$

Knowing the contact forces for a given object pose, the friction cone stability criteria can be assessed to check whether that object pose lies within the frictionally stable (or, grasp stable) workspace of the hand. In this model, a conservative maximal possible static friction coefficient of $\mu_{max} = 1$ was chosen between rubber fingerpads and a solid object [36], [37].

Hand designs with different parameters can be compared for the number of frictionally stable poses within their workspace, and the optimal parameters can be identified that maximize this workspace size. Since the actuator forces transmitted through the fingers depend heavily on the link lengths, the L_1 parameter was first discretized and explored in the design space. To normalize the size of the hand, the value of L_1 was divided by the radius of the sphere (R_{sph}) that the contacts lie on. Note that the link 2 length can be calculated as L_2=sqrt($R_{sph}{}^2 - L_1{}^2$), and is thus not an independent parameter in the search space. Different hand configurations with $L_1/R_{sph} \in [0.05, 0.95]$ were simulated, and over 1000 multi-DOF poses were tested for kinematic and frictional stability. The fraction of these workspace poses that satisfied the friction stability criteria as a function of the normalized link 1 length is shown in Fig. 3. The drop in workspace size for higher L_1/R_{sph} values is in part due to the ±90° joint limit placed on the R2 joint required for a physical implementation. The largest fraction of frictionally stable poses with $\mu_{max} = 1$ was 0.64 and corresponds to an optimal value of $L_1/R_{sph} = 0.5$.

The initial angle of the R2 joint ($\beta_{init,i}$) did not seem to affect the friction stability of a pose especially for smaller

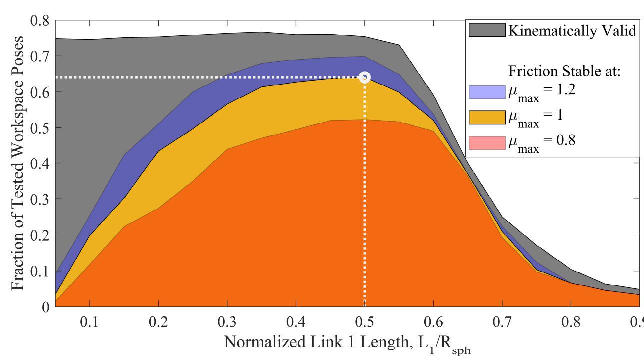

Fig. 3. Fraction of the kinematically valid and frictionally stable workspace as a function of the normalized length of link 1. A maximum static friction coefficient expected at the contacts of $\mu_{max} = 1$ is chosen, and the link 1 length corresponding to the largest frictionally stable workspace for this coefficient value is noted to be at $L_1/R_{sph} = 0.5$.

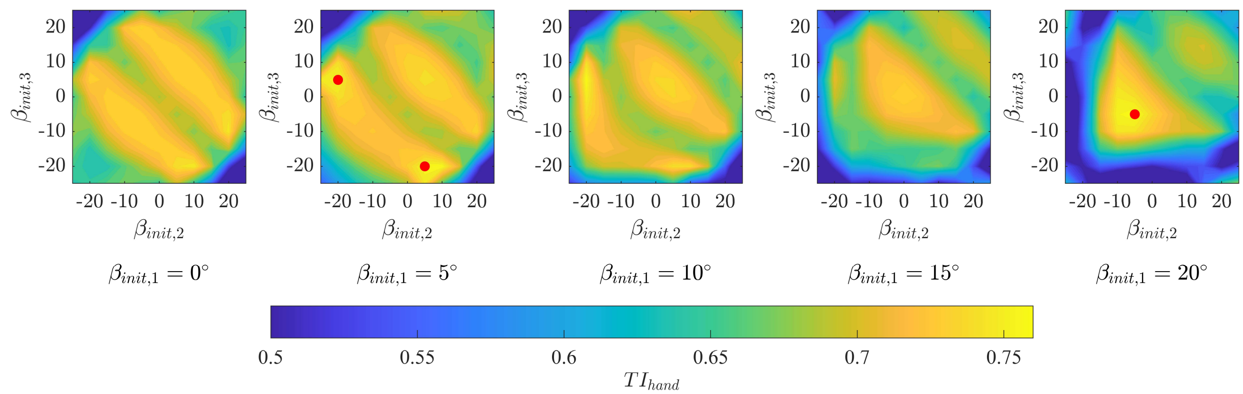

Fig. 4. Variation in the average adapted Transmission Index (TI_{hand}) across the hand's workspace as a function of initial R2 joint angle ($\beta_{init,i}$) at the 3 fingers. Each column of the plot corresponds to a slice taken at a positive value of finger 1's initial R2 joint angle ($\beta_{init,1}$) while those for finger 2 ($\beta_{init,2}$) and finger 3 ($\beta_{init,3}$) are varied. The red dots indicate the design configurations with the maximum value of the average TI_{hand}. Note that the configurations identified by these dots are simply rotated versions of one another, and are thus kinematically similar.

angles, because it does not change the moment arm of the actuators nearly as much as the link lengths do. So, $\beta_{init,i} = 0$ was used for the different link lengths tested above. However, the optimal values for $\beta_{init,i}$ from the following section were still confirmed for size of their frictionally stable workspace, and found to be 0.63x of the all the poses tested. As mentioned before, the largest size of workspace with $\beta_{init,i} = 0$ and the same link lengths was 0.64x of all the poses tested.

The link length optimization conducted here only indicates if a particular object pose is stable within the hand, but does not signal if the fingers can transmit appropriate forces to reach the desired poses within the hand's workspace. In other words, grasp stability of a pose does not guarantee manipulability of the hand to orient the object to that particular pose. The following motion quality metric accounts for this aspect of the manipulation by looking at hand-object system's singularities.

B. Motion Quality from Adapted Transmission Index

To test the manipulability of the hand through the frictionally stable workspace determined previously, we adopt the *local transmission index* (LTI) formulation proposed in [38] with some key modifications to adapt the index from a parallel manipulator context to a hand-object setting. The LTI is typically calculated at each pose, and ranges from 0 (singular pose) to 1 (ideal motion/force transmissibility). Other manipulability metrics have been proposed [39], [40], but the LTI metric was chosen for its frame-free representation, unit independence, and singularity type identification properties. Moreover, the index could also be easily adapted to a robot hand as described below.

The LTI of a parallel manipulator is defined as the minimum of 2 sub-metrics computed for each leg—input (λ_i) and output (η_i) transmission indices for i^{th} leg.

$$\lambda_i = \frac{|\$_{T_i} \circ \$_{I_i}|}{|\$_{T_i} \circ \$_{I_i}|_{\max}}, \eta_i = \frac{|\$_{T_i} \circ \$_{O_i}|}{|\$_{T_i} \circ \$_{O_i}|_{\max}}$$
$$\mathrm{LTI} = \min(\eta_i, \lambda_i) \quad (3)$$

where $\$_{I_i}$ is the input twist screw from i^{th} actuator, $\$_{T_i}$ is the transmission wrench screw exerted by i^{th} leg on the end effector, and $\$_{O_i}$ is the output twist screw of motion allowed when all legs are locked and only the i^{th} actuator is moved.

For our 3-RRS configuration, the derivations for these unit screws can be referenced from the spherical parallel manipulator example in [38]. However, the LTI metric does not discriminate transmission capability of fingers that are applying forces in opposite direction to the motion of the contact/object, nor does it consider the friction cone requirement on the contact forces of a hand-object system, since it is not present in parallel platforms. While the grasp stability criteria ensures that we only consider poses where fingers push and apply friction on the object surface, we also need to identify force transmissibility only from fingers that are applying forces in direction of the object motion. So, an adapted transmission index (TI_{hand}) is proposed here which, instead of taking the minimum of input and output indices from all legs, only considers the indices from fingers that do positive work ($W_{f,i}$) on the object. This work was defined as the dot product of the displacement of the fingertip (d_i) with the fingertip contact force ($f_{c,i}$).

$$TI_{hand} = \min(\eta_i, \lambda_i : W_{f,i} > 0) \quad i \in [1,3]$$
$$\text{where,} \quad W_{f,i} = f_{c,i} \cdot d_i \quad (4)$$

The overall motion quality of a hand was then calculated by taking the average of TI_{hand} from all the frictionally stable poses in that hand's workspace. Recall that this metric primarily highlights the motion/force transmissibility of a design configuration by virtue of avoiding singularities. Changing the link lengths does not circumvent the Type 2 (or rotational) singularities that this spherical parallel mechanism encounters [25], [41]. The initial angle at the R2 joint ($\beta_{init,i}$) needs to be altered for the 3 fingers to improve the motion quality metric.

A total of 1331 hand designs with different combinations of $\beta_{init,i} \in [-25°, 25°]$ and a 5° step size for each finger were simulated for their workspaces' motion qualities, and some of these results are shown in Fig. 4. The equilateral contact triangle constraint established prior to the optimization process was satisfied by rotating the actuator axes about the fixed center in the plane of the palm, so that the resulting contact points still formed an equilateral triangle. Plots for only $\beta_{init,1} > 0$ are shown, because the remaining designs are simply their mirrored versions. From the results, the configurations with the highest motion quality were identified to be mirrored or rotationally similar versions of $\beta_{init} = [20°, -5°, -5°]$.

IV. MECHANICAL IMPLEMENTATION

The optimal parameters determined in the previous section were implemented in a prototype hand in order to run physical experiments validating the performance of a 3-RRS spherical parallel platform-based hand indicated by the simulation results. An $R_{sph} = 100$ mm was arbitrarily chosen to define the overall size of the hand. The spherical joint on each leg would simply be a point contact with friction as modeled in the prior sections, however the implementation of the 2 revolute joints (one active and one passive) is not as straightforward and is described below. The design of each finger alongside the design parameters is detailed in Fig. 2 (b), and the whole hand assembly is shown in Fig. 5 (a).

To create enough space for the actuators connected to the active R1 joints on each finger, a spur-internal gear transmission was opted for that situated the actuator further away from the fixed center. Any point on the internal gear rotates about the axis of the gear, and thus behaves identical to a revolute joint. The R2 joint is implemented with a conventional dowel pivoting on bearings. Extension return springs were added to either side of the R2 joints on each finger to hold the joint in position while the hand grasped an object. Without these springs and the assumption of a fixed R2 joint angle at grasp, the fingertip positions would be indeterminate, and subsequently the object could not be manipulated without an inverse kinematics model of the hand-object system. However, these springs also needed to be light enough to allow the joint to passively rotate under the action of grasping and actuator forces during manipulation. Large spring forces could prevent the R2 joint from rotating and cause fingertip slipping on the surface of the object.

Since only the axis of the gear is critical to the fixed center location, the 3 fingers were equipped with internal gears of 3 different radii. This was done to allow the gears to layer on top of each other and prevent interference, thus allowing for a larger sector angle on each gear and consequently, a larger range of motion for the R1 joint. Circular tracks (shown in yellow in Fig. 5 (a)) with radii corresponding to their respective internal gear were mounted to the bottom plate and constrained the R1 axes. The top plate provided a flat palm surface for the hand and isolated the gear components from the objects above. The actuator torque at each finger was calculated to match the grasping forces after accounting for the differing gear ratios. The hand was designed to be fabricated from 3D printed ABS parts and off-the-shelf components such as extension springs, standoffs, bearings, and actuators (Dynamixel XM430-W350-R). Although the fingertip was previously modeled as a point contact with friction, the fingertip area was increased slightly to improve friction properties and adhesive rubber pads were also added to meet the static friction coefficient value used in Section III. Ball joints were briefly tested at the fingertips to mimic a spherical joint more exactly, and showed similar performance to static fingertips. They were not included in the final design due to their notably higher weight and size, especially for versions with a large swivel angle. A more in-depth study comparing different fingertips to the point contact with friction model will be conducted in the future.

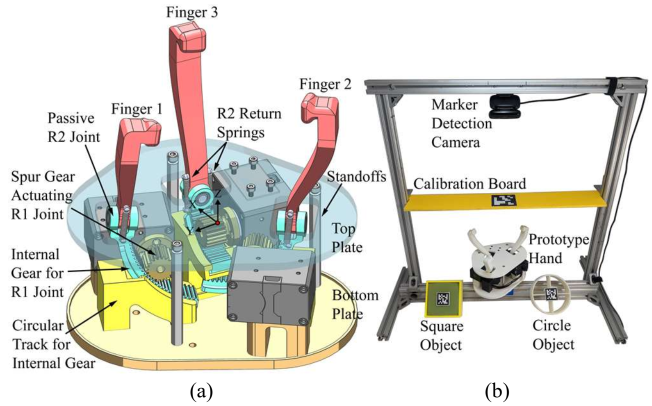

Fig. 5. (a) Prototype hand's components are labeled on a rendered CAD assembly of the design. (b) Experimental test setup with the prototype hand mounted on a frame used for characterization of the hand's actual manipulation workspace. The removable yellow calibration board sets the global coordinate frame for the camera.

V. EXPERIMENTAL RESULTS

The proof-of-concept hand prototype was experimentally validated through a series of grasping tests, manipulation characterizations, and a real-world task to evaluate the approach of adapting spherical parallel platforms to robot hands. These experiments validated grasp generation on a variety of objects, manipulation along the three rotation axes, conformity of the measured object poses to the predicted manipulation sphere, and ability of this hand architecture to execute real-world tasks. For the tests in Section V.B-C, two objects (a circular object with a diameter of 100 mm, and a square object with a side length of 90 mm) were tagged with ArUco markers [42], and the hand was mounted on a frame with a fixed camera pointing at the palm (Fig. 5 (b)).

Once an object was grasped, the hand-object system behaved akin to a 3-RRS parallel platform, where the shape of the movable platform could be calculated based on the actuator positions at grasp and initial angle of the passive R2 joints. Within-hand manipulation was then carried out by way of purely open-loop position commands sent to the actuators determined from the inverse kinematics of the hand-object system. The non-overconstrained nature of the mechanism ensured that the object was not dropped even with simple open-loop control schemes. The detected marker pose was recorded but not used for any feedback control.

A. Generating Grasps on YCB Objects

The first step of any robot manipulation task is to obtain a robust grasp on the object. We evaluate the grasping capability of our robot hand with 9 objects of various shapes and sizes selected from the YCB Object and Model Set [43]. One of the issues encountered by the spherical hand topologies in [11] was low grasp force output due to the curved fingers, which did not direct forces to the center of the hand. We wanted to validate the grasping performance of our hand on objects with a wide variety of profiles in the plane. The 3 actuators were operated in torque control mode in order to grasp without prior knowledge of object geometries. The R2 joints were observed to stay at the same initial angle during grasp, allowing the contact locations to be estimated based on actuator positions. The 9 objects grasped with the hand are shown in Fig. 6.

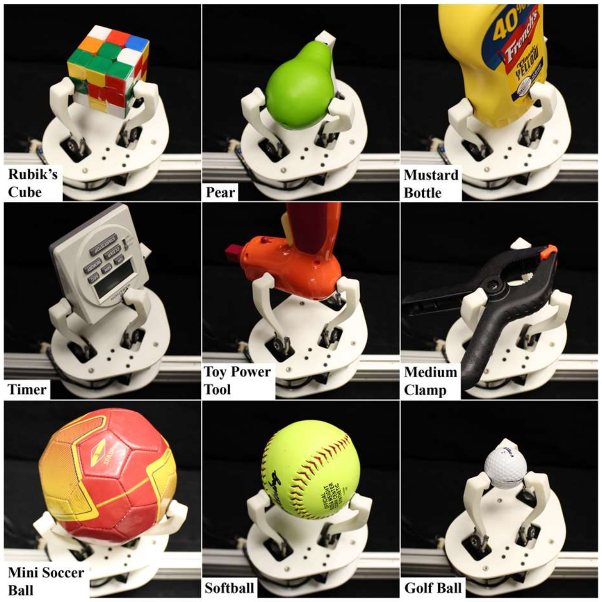

Fig. 6. Grasping performance of the prototype hand on 9 YCB objects. The objects were held approximately at the home position, while the actuators closed the fingers around the object in torque control mode.

Even though this prototype hand successfully generated robust grasps on a range of object sizes, the subsequent manipulation range of motion was restricted by the sector angle of the internal gears, especially for very large (e.g., mini soccer ball) or very small objects (e.g., golf ball). The gears' sector angle could not be increased beyond about 80° due to interferences with adjacent assembly components. Note that this stems from the prototype's mechanical design—the underlying hand architecture should still be able to manipulate any object geometry. Future work on the design will consider alternate transmission methods to evaluate the manipulation performance with a wide array of object geometries.

B. Single-axis Characterization

The 100 mm diameter circle object was used to characterize the manipulation performance of the hand along the 3 rotation axes individually. The circular cross-section of the object allowed similarity across consecutive grasps of the object. Once the object was grasped at the zero position, the 3 actuators are commanded to rotate the object to the kinematic end of range of the motion along the roll (about X in Fig. 5 (a)), pitch (about Y), and yaw (about Z) axes separately, while the camera detected the actual orientation of the object. These poses for 5 trials on each of the 3 axes are shown alongside the theoretically expected orientation of the object in Fig. 7.

Rotations about the 3 axes are similarly precise within the range of motion set by the design constraints. Especially within 20° of the starting position, the roll, pitch, and yaw motions are accurate for most physical applications. The object was observed to stay within the grasp of the hand throughout all the trials in each axes' testing, and the passive R2 joint rotated as expected under the effect of grasp and actuator forces. The assumption of fixed R2 joint angle at grasp in order to estimate the fingertip locations seemed to have been justified, as the hand-object system's inverse kinematics utilizing these locations effectively estimated the grasped object's pose between the fingertips.

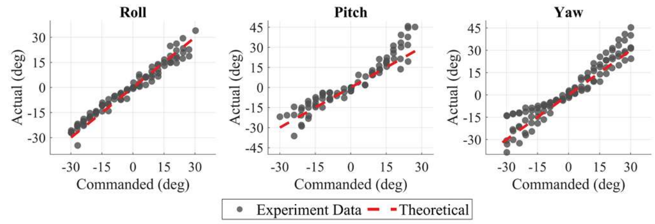

Fig. 7. Single axis characterization results with the circle object manipulated through the kinematic range of motion along the 3 rotational axes. The object's actual pose is detected across 5 trials on each axis. The theoretical line indicates a case where commanded and actual poses match exactly.

Deviation from the theoretically expected orientation of the object towards the end of these ranges occurred primarily due to the object slipping at the fingertips. Even though there might be sufficient grasping force at the fingertips, larger rotations also require the return springs at the R2 joints to extend more, increasing the resistance of this joint to passively rotate under actuator and grasp forces. Much lighter return springs were tested as an alternative, however the R2 joint could not be held fixed during the grasping process as contact forces would change this joint angle and lead to an incorrect estimate of the contact point location. In future work, brakes for locking this joint prior to manipulation as well as higher friction finger pads will be explored.

C. Spherical Surface Fit of Actual Manipulation Workspace

While the single-axis characterizations are helpful to quantify the performance of the hand in each of three rotation directions, it is important to evaluate if the object manipulates on the sphere promised by the intersecting revolute axes of this design architecture. In order to confirm if the hand rotates the object about a fixed point, we commanded 2 objects (square and circle) to 130 points each in the roll and pitch workspace of the hand, and recorded the actual object positions. The mean squared error between these points and their Z-projections on the theoretical sphere of manipulation was reported after normalizing by the radius of the manipulation sphere (in Fig. 8, this error is denoted as $\widehat{\mathrm{MSE}}$ and has units of mm). The ArUco marker on the objects were used to detect the actual position of the objects' centroids as they were manipulated to different roll and pitch combinations. Yaw rotations would not move the object's centroid in 3D space and were thus not included in this test. The square and circle object positions overlayed on the manipulation sphere that they would be expected to lie on are shown in Fig. 8.

The hand appears to grasp and manipulate the square object just as well as the circle shaped object, and there is no discernible difference between the errors of their respective object centroids to the sphere ($\widehat{\mathrm{MSE}}_{\mathrm{square}} = 0.0203$, $\widehat{\mathrm{MSE}}_{\mathrm{circle}} = 0.0219$). The overall error ($\widehat{\mathrm{MSE}} = 0.0211$) of all the points is low considering the hand adds a strict friction stability requirement, which is absent in the equivalent parallel platform version. The points falling furthest from the sphere are at larger rotations due to similar effects seen in Section V.B, while object positions near the Z-axis conformed more closely to the sphere ($\widehat{\mathrm{MSE}}_{\|\mathrm{angle}\|<20^\circ} = 0.0121$). Since smaller rotations are more accurate and fit the sphere better, manipulation motions can be restricted within this range but carried out over more iterations by releasing and regrasping the object. This gaiting manipulation strategy and the utility of

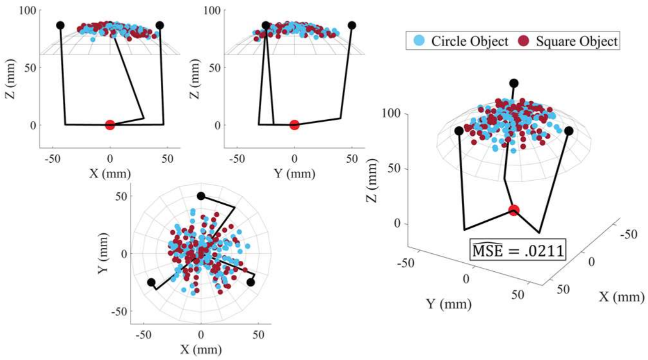

Fig. 8. Actual detected position of circle and square objects is overlayed on a spherical surface that the object's centroid should theoretically stay on. The red dot denotes the sphere's center, where fingers' revolute axes converge.

this spherical parallel platform architecture in real-world scenarios was evaluated in the following section.

D. Screwing In a Lightbulb

Most real-world tasks would require a hand to carry out coupled rotations along multiple axes, particularly when the robot arm is constrained by the environment and cannot align in such a way that the hand only needs to manipulate the object along one of those DOFs. We simulate such a scenario by executing the task of screwing in a lightbulb mounted at 2 different angles. A simple screwing motion primarily uses the yaw motion i.e., rotation about the Z-axis of the hand, but by tilting the socket's screw axis, we require the hand to perform such rotations about a different axis passing through the fixed center, thus validating multi-DOF spherical manipulation abilities of the hand.

To maintain the realistic characteristics of this task, a commercially available lightbulb of 60 mm diameter was sourced. While an object of this smaller size could be grasped by the hand, the internal gears for R1 joint did not have sufficient range of motion left post-grasp to carry out large manipulation motions. As a result, a scaled down version of the hand was used for this task by reducing the R_{sph} parameter from 100 mm down to 60 mm, and L_1 down from 50 mm to 30 mm (in order to maintain the optimal $L_1/R_{sph} = 0.5$). Other dependent length parameters were scaled down accordingly. The physical design of this hand simplified the process of scaling down the hand by only needing to swap out the pink links on the three fingers from Fig. 5 (a).

In order to maintain brevity and exemplify the concept, the bulb starts in a partially screwed in but disconnected position. It still requires over 45° of turning to be successfully screwed in and lit up. Subsequently, the hand needs to release the bulb at hard stops, regrasp, and manipulate the bulb multiple times—akin to how a human would perform the same task. Fig. 9 shows a sequence of images during this task. The screw axis of the bulb is known beforehand but subsequent rotation motions about that axis are carried out open-loop until the human operator decides the bulb is sufficiently screwed in and lit up, at which point the operator ends the task. The hand is able to successfully connect the bulb after 2-3 regrasps interspersed by manipulations as shown in Fig. 9.

The glass surface of a light bulb is very smooth and easily susceptible to slip. This challenge is compounded by the increasing friction as the bulb screws in further into the socket.

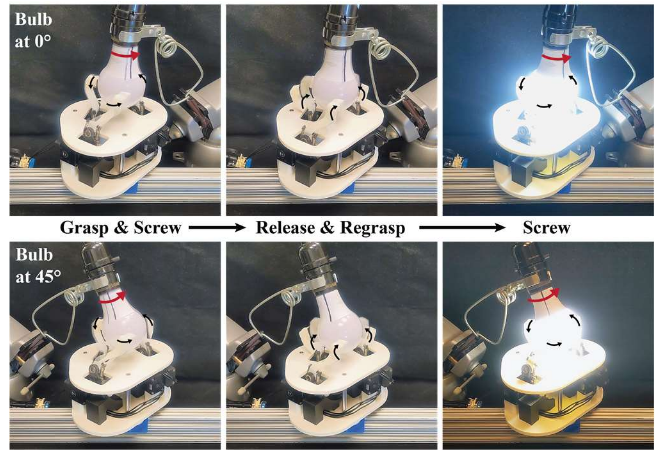

Fig. 9. Screwing in a light bulb mounted at 2 different angles through a sequence of motions about the bulb's axis. When the fingers reach their hard stops, the bulb is released, regrasped, and rotated again until it lights up.

As a result, the inverse kinematics and open-loop control of the hand-object system would often underestimate the number of turns required to connect the bulb due to effects from slippage and return spring forces. Consequently, closing the feedback loop (in this case, with a human operator) is beneficial to completing the task. While the goal of this work was not to develop control schemes for the hand, future work will consider incorporating feedback mechanisms in the hand.

VI. Discussion and Future Work

In this paper we presented a 3-fingered hand based on the 3-RRS spherical parallel platform architecture capable of manipulating the grasped object about a fixed point. The revolute axes of the fingers converge at this point, and along with the fingertips modeled as point contact with friction, this results in an exactly constrained hand-object system that is simple to control. The hand architecture was optimized for a large workspace area that could be explored with a stable grasp and without encountering singularities. Optimal design parameters resulting from this framework were used to prototype a physical implementation of this hand architecture. And, finally, experimental results from grasping tests, manipulation characterization, and real-world task scenarios showed that the hand was able to generate grasps on a range of object shapes and perform precise rotations about one or multiple axes. Such a dexterous hand capable of executing rotations about all 3 axes can replace the need for a wrist on a robot arm, and significantly augment functionality of low-DOF arms and translational stages.

Future work on the hand will look into reducing slip effects at the fingertips. The extension springs used in this prototype stabilized the R2 joint at grasp, but also applied counter forces during manipulation at large object rotations. First, alternative approaches to avoiding indeterminacy of this joint angle will be explored, including adding a secondary actuator, or friction brake at the joint. Second, encoders or potentiometers would be considered to be added to this joint in order to make the estimation of the fingertip location even more robust. Lastly, tactile feedback sensors on the fingertips could also aid grasp and slip detection during manipulation. Overall, the authors believe parallel platform-based hand architectures can inspire more dexterous hands as evidenced from our results, and thus warrant further exploration.

References

[1] R. R. Ma and A. M. Dollar, “On dexterity and dexterous manipulation,” in *2011 15th International Conference on Advanced Robotics (ICAR)*, Jun. 2011, pp. 1–7, doi: 10.1109/ICAR.2011.6088576.

[2] M. Grebenstein *et al.*, “The DLR hand arm system,” *Proc. - IEEE Int. Conf. Robot. Autom.*, pp. 3175–3182, 2011, doi: 10.1109/ICRA.2011.5980371.

[3] E. N. Gama Melo, O. F. Avilés Sánchez, and D. Amaya Hurtado, “Anthropomorphic robotic hands: a review,” *Ing. y Desarro.*, vol. 32, no. 2, pp. 279–313, Jun. 2014, doi: 10.14482/inde.32.2.4715.

[4] Z. Xu and E. Todorov, “Design of a highly biomimetic anthropomorphic robotic hand towards artificial limb regeneration,” *Proc. - IEEE Int. Conf. Robot. Autom.*, vol. 2016-June, pp. 3485–3492, 2016, doi: 10.1109/ICRA.2016.7487528.

[5] A. Bicchi, “Hands for dexterous manipulation and robust grasping: a difficult road toward simplicity,” *IEEE Trans. Robot. Autom.*, vol. 16, no. 6, pp. 652–662, 2000, doi: 10.1109/70.897777.

[6] A. Bicchi and A. Marigo, “Dexterous grippers: Putting nonholonomy to work for fine manipulation,” *Int. J. Rob. Res.*, vol. 21, no. 5–6, pp. 427–442, 2002, doi: 10.1177/027836402321261968.

[7] S. Yuan, L. Shao, C. L. Yako, A. Gruebele, and J. K. Salisbury, “Design and control of roller grasper V2 for in-hand manipulation,” in *2020 IEEE/RSJ International Conference on Intelligent Robots and Systems (IROS)*, 2020, pp. 9151–9158, doi: 10.1109/IROS45743.2020.9340953.

[8] M. Higashimori, H. Jeong, I. Ishii, M. Kaneko, A. Namiki, and M. Ishikawa, “A new four-fingered robot hand with dual turning mechanism,” *Proc. - IEEE Int. Conf. Robot. Autom.*, vol. 2005, no. April, pp. 2679–2684, 2005, doi: 10.1109/ROBOT.2005.1570518.

[9] R. R. Ma and A. M. Dollar, “An underactuated hand for efficient finger-gaiting-based dexterous manipulation,” in *2014 IEEE International Conference on Robotics and Biomimetics (ROBIO 2014)*, Dec. 2014, pp. 2214–2219, doi: 10.1109/ROBIO.2014.7090666.

[10] B. Eldridge *et al.*, “A remote center of motion robotic arm for computer assisted surgery,” *Robotica*, vol. 14, no. 1, pp. 103–109, Jan. 1996, doi: 10.1017/S0263574700018981.

[11] R. R. Ma, N. Rojas, and A. M. Dollar, “Spherical hands: Toward underactuated, in-hand manipulation invariant to object size and grasp location,” *J. Mech. Robot.*, vol. 8, no. 6, pp. 1–12, 2016, doi: 10.1115/1.4034787.

[12] J. Borràs and A. M. Dollar, “Analyzing dexterous hands using a parallel robots framework,” *Auton. Robots*, vol. 36, no. 1–2, pp. 169–180, Jan. 2014, doi: 10.1007/s10514-013-9380-x.

[13] J. S. Dai, Delun Wang, and L. Cui, “Orientation and Workspace Analysis of the Multifingered Metamorphic Hand—Metahand,” *IEEE Trans. Robot.*, vol. 25, no. 4, pp. 942–947, Aug. 2009, doi: 10.1109/TRO.2009.2017138.

[14] J. Sun, X. Zhang, G. Wei, and J. S. Dai, “Geometry and kinematics for a spherical-base integrated parallel mechanism,” *Meccanica*, vol. 51, no. 7, pp. 1607–1621, 2016, doi: 10.1007/s11012-016-0438-7.

[15] C. M. McCann and A. M. Dollar, “Design of a stewart platform-inspired dexterous hand for 6-DOF within-hand manipulation,” in *2017 IEEE/RSJ International Conference on Intelligent Robots and Systems (IROS)*, Sep. 2017, pp. 1158–1163, doi: 10.1109/IROS.2017.8202287.

[16] C. M. Gosselin and J.-F. Hamel, “The agile eye: a high-performance three-degree-of-freedom camera-orienting device,” in *Proceedings of the 1994 IEEE International Conference on Robotics and Automation*, 1994, pp. 781–786, doi: 10.1109/ROBOT.1994.351393.

[17] C. Gosselin and J. Angeles, “The Optimum Kinematic Design of a Spherical Three-Degree-of-Freedom Parallel Manipulator,” *J. Mech. Transm. Autom. Des.*, vol. 111, no. 2, pp. 202–207, Jun. 1989, doi: 10.1115/1.3258984.

[18] M. C. Palpacelli, L. Carbonari, G. Palmieri, and M. Callegari, “Analysis and Design of a Reconfigurable 3-DoF Parallel Manipulator for Multimodal Tasks,” *IEEE/ASME Trans. Mechatronics*, vol. 20, no. 4, pp. 1975–1985, 2015, doi: 10.1109/TMECH.2014.2365616.

[19] C. Innocenti and V. Parenti-Castelli, “Echelon form solution of direct kinematics for the general fully-parallel spherical wrist,” *Mech. Mach. Theory*, vol. 28, no. 4, pp. 553–561, Jul. 1993, doi: 10.1016/0094-114X(93)90035-T.

[20] K. Wohlhart, “Displacement analysis of the general spherical Stewart platform,” *Mech. Mach. Theory*, vol. 29, no. 4, pp. 581–589, May 1994, doi: 10.1016/0094-114X(94)90096-5.

[21] R. Di Gregorio, “Kinematics of a new spherical parallel manipulator with three equal legs: The 3-URC wrist,” *J. Robot. Syst.*, vol. 18, no. 5, pp. 213–219, May 2001, doi: 10.1002/rob.1017.

[22] R. Di Gregorio, “A new parallel wrist using only revolute pairs: the 3-RUU wrist,” *Robotica*, vol. 19, no. 3, pp. 305–309, May 2001, doi: 10.1017/S0263574700003192.

[23] X. Kong and C. M. Gosselin, “Type synthesis of three-degree-of-freedom spherical parallel manipulators,” *Int. J. Rob. Res.*, vol. 23, no. 3, pp. 237–245, 2004, doi: 10.1177/0278364904041562.

[24] A. Chaker, A. Mlika, M. A. Laribi, L. Romdhane, and S. Zeghloul, “Clearance and manufacturing errors’ effects on the accuracy of the 3-RCC Spherical Parallel Manipulator,” *Eur. J. Mech. - A/Solids*, vol. 37, pp. 86–95, Jan. 2013, doi: 10.1016/j.euromechsol.2012.05.009.

[25] R. Di Gregorio, “The 3-RRS Wrist: A New, Simple and Non-Overconstrained Spherical Parallel Manipulator,” *J. Mech. Des.*, vol. 126, no. 5, pp. 850–855, Sep. 2004, doi: 10.1115/1.1767819.

[26] M. Karouia and J. M. Hervé, “An Orientational 3-dof Parallel Mechanism,” *Proc. 3rd Chemnitz Parallel Kinemat. Semin.*, no. January 2002, pp. 23–25, 2002.

[27] X. Kong and C. M. Gosselin, “Type Synthesis of 3-DOF Spherical Parallel Manipulators Based on Screw Theory,” *J. Mech. Des. Trans. ASME*, vol. 126, no. 1, pp. 101–108, 2004, doi: 10.1115/1.1637655.

[28] H. Tetik and G. Kiper, “A geometrical approach for the singularity analysis of a 3-RRS parallel manipulator,” *Mech. Mach. Sci.*, vol. 50, pp. 349–356, 2018, doi: 10.1007/978-3-319-60867-9_40.

[29] Jianfeng Li, Jinsong Wang, Wusheng Chou, Yuru Zhang, Tianmiao Wang, and Qixian Zhang, “Inverse kinematics and dynamics of the 3-RRS parallel platform,” in *Proceedings 2001 ICRA. IEEE International Conference on Robotics and Automation (Cat. No.01CH37164)*, 2001, vol. 3, pp. 2506–2511, doi: 10.1109/ROBOT.2001.932999.

[30] K. H. Hunt, *Kinematic Geometry of Mechanisms*. Oxford University Press in Oxford, New York, 1978.

[31] C. . Tischler, A. . Samuel, and K. . Hunt, “Kinematic chains for robot hands—II. Kinematic constraints, classification, connectivity, and actuation,” *Mech. Mach. Theory*, vol. 30, no. 8, pp. 1217–1239, Nov. 1995, doi: 10.1016/0094-114X(95)00044-Y.

[32] J. P. Merlet, *Parallel Robots*, vol. 128. Berlin/Heidelberg: Springer-Verlag, 2006.

[33] R. Kelaiaia, A. Zaatri, O. Company, and L. Chikh, “Some investigations into the optimal dimensional synthesis of parallel robots,” *Int. J. Adv. Manuf. Technol.*, vol. 83, no. 9–12, pp. 1525–1538, Apr. 2016, doi: 10.1007/s00170-015-7611-3.

[34] C. M. McCann and A. M. Dollar, “Analysis and Dimensional Synthesis of a Robotic Hand Based on the Stewart-Gough Platform,” in *Volume 5A: 42nd Mechanisms and Robotics Conference*, Aug. 2018, pp. 1–8, doi: 10.1115/DETC2018-86149.

[35] R. M. Murray, Z. Li, and S. S. Sastry, *A Mathematical Introduction to Robotic Manipulation*. CRC Press, 1994.

[36] W. G. Bircher, A. M. Dollar, and N. Rojas, “A two-fingered robot gripper with large object reorientation range,” in *2017 IEEE International Conference on Robotics and Automation (ICRA)*, May 2017, pp. 3453–3460, doi: 10.1109/ICRA.2017.7989394.

[37] E. Oberg, *Machinery’s Handbook*. Industrial Press, 2012.

[38] J. Wang, C. Wu, and X. J. Liu, “Performance evaluation of parallel manipulators: Motion/force transmissibility and its index,” *Mech. Mach. Theory*, vol. 45, no. 10, pp. 1462–1476, 2010, doi: 10.1016/j.mechmachtheory.2010.05.001.

[39] T. Yoshikawa, “Manipulability of Robotic Mechanisms,” *Int. J. Rob. Res.*, vol. 4, no. 2, pp. 3–9, Jun. 1985, doi: 10.1177/027836498500400201.

[40] J. P. Merlet, “Jacobian, Manipulability, Condition Number, and Accuracy of Parallel Robots,” *J. Mech. Des.*, vol. 128, no. 1, pp. 199–206, Jan. 2006, doi: 10.1115/1.2121740.

[41] C. Gosselin and J. Angeles, “Singularity analysis of closed-loop kinematic chains,” *IEEE Trans. Robot. Autom.*, vol. 6, no. 3, pp. 281–290, Jun. 1990, doi: 10.1109/70.56660.

[42] S. Garrido-Jurado, R. Muñoz-Salinas, F. J. Madrid-Cuevas, and R. Medina-Carnicer, “Generation of fiducial marker dictionaries using Mixed Integer Linear Programming,” *Pattern Recognit.*, vol. 51, pp. 481–491, 2016, doi: 10.1016/j.patcog.2015.09.023.

[43] B. Calli, A. Walsman, A. Singh, S. Srinivasa, P. Abbeel, and A. M. Dollar, “Benchmarking in Manipulation Research: Using the Yale-CMU-Berkeley Object and Model Set,” *IEEE Robot. Autom. Mag.*, vol. 22, no. 3, pp. 36–52, Sep. 2015, doi: 10.1109/MRA.2015.2448951.